

# Anisotropic soft X-ray emission spectroscopy study of the valence electron state of $\text{Lu}(\text{Al}, T)\text{B}_4$ ( $T = \text{Cr}, \text{Mn}, \text{Fe}, \text{Mo}$ ) exhibiting two-dimensional B-layers

Yuki Hada<sup>1</sup>, Yuda Hatakeyama<sup>1</sup>, Yohei K. Sato<sup>1</sup>, Masami Terauchi<sup>1,2\*</sup>, Kaoru Kouzu<sup>3</sup>, and Shigeru Okada<sup>4</sup>

<sup>1</sup>IMRAM, Tohoku University, Sendai 980-8577, Japan

<sup>2</sup>AMA Co-Creation Research Center, Tohoku University, Sendai 980-8577, Japan

<sup>3</sup>Department of Science and Engineering, Kokushikan University, Tokyo 154-8515, Japan

<sup>4</sup>Research Institute for Engineering, Kanagawa University, Yokohama 221-8686, Japan

**Abstract.**  $\text{Lu}(\text{Al}, T)\text{B}_4$  ( $T = \text{Cr}, \text{Mn}, \text{Fe}, \text{Mo}$ ) have the alternate stacking structure of B-layer and  $\text{Lu}(\text{Al}, T)$ -layer along the  $c$ -axis. B-K emission spectra of these materials are measured at two take-off angles of  $20^\circ$  and  $70^\circ$  from the  $c$ -plane. The energy region corresponding to the top of valence band (VB) shows a larger spectrum intensity at the smaller take-off angle, responsible for  $p_z$  character. The bottom region shows the opposite angle dependence, responsible for  $p_x$  and  $p_y$  character. The middle of the VB of a large peak intensity shows almost no angle dependence, suggesting an isotropic distribution of bonding charge. As a whole, the angle-dependence of the B-K emission intensity is smaller than that of graphite. This rather isotropic bonding-charge distribution of the boron-layer can make the inter-layer bonding between B-layer and adjacent  $\text{Lu}(\text{Al}, T)$  layer and is presumably related to the hardness of those bulk materials.

## 1 Introduction

Spectroscopic methods based on electron microscopy are indispensable to explore the electronic structure of local specimen areas below the micrometer level. Among these analytical methods, soft X-ray emission spectroscopy (SXES), which is known as a tool for investigating the electronic structure of solids [1], combined with electron microscopy not only enables elemental analysis but also provides the information of the energy state of valence electrons of assigned specimen areas [2,3]. Furthermore, SXES coupled with electron microscopy has succeeded in visualizing the spatial distribution of chemical bonding states in heterogeneous materials [4-6].

---

\* Corresponding author: [m\\_terauchi@tohoku.ac.jp](mailto:m_terauchi@tohoku.ac.jp)

It has been known that the direction of X-ray emission is affected by the distribution of the bonding electrons [7]. Anisotropic SXES measurements using a synchrotron radiation facility and an SXES electron microscope have been reported for crystals with anisotropic structures such as graphite and *h*-BN [2,8]. Recently, anisotropic SXES measurements for a superconductor NaAlSi having Al-Si layers composed of  $sp^3$  bonding [9] and a graphite related material of  $MgB_2C_2$  with B-C honeycomb layers [10] were reported, in which the bonding character was discussed by comparing the experimental emission profile with calculated partial density of states of the valence band (VB).

Boron and boron-rich compounds forms not only boron-polyhedral-unit based clusters ( $B_6$  and  $B_{12}$  clusters) but also two-dimensional (2D) boron-sheet based structures [11]. Since the finding of the superconducting nature of  $MgB_2$  having 2D boron-honeycomb-layers [12], the related structured materials of carbon-doped  $MgB_2$  [13] and  $MgB_2C_2$  [14] were investigated. These materials are based on 2D B-C honeycomb-layer structures related to graphite. Boron forms another type of 2D sheet composed of 5, 6, and 7 membered-rings.  $REAlB_4$  (RE: rare earth element) is one of the ternary RE-Al-B system.  $REAlB_4$  has a metallic nature and two types of structures with different arrangements of 5 and 7-membered rings in 2D-boron-layer;  $YCrB_4$ -type (a-type, space group:  $Pbam$ ) and  $ThMoB_4$ -type (b-type, space group:  $Cmmm$ ) [15].  $YCrB_4$ -type crystal of  $TmAlB_4$  has recently attracted much attention because an antimagnetic transition was found with  $T_N=5.5$  K [16]. Furthermore, interesting electronic and physical properties, such as the possibility of controlling thermal conductivity through structural defects and its use as a high-temperature thermoelectric material, were reported [17,18]. In addition, the improvement of thermoelectric properties by the introduction of magnetic ions and other elements has recently attracted attention [19]. Due to that, syntheses of  $YCrB_4$ -type crystals introduced magnetic ions of  $Lu(Al,T)B_4$  ( $T=Cr, Fe, Mo, Mn$ ) [20,21] and  $Yb(Al,T)B_4$  ( $T=Cr, Fe, Mo, W$ ) [22,23] were conducted and reported the dependence of lattice constants, micro-Vickers hardness, and magnetic susceptibility on introduced magnetic ions. The reported dependence of physical properties should be related to the chemical bonding nature of the material. However, the spectroscopic evaluation of those materials has not been reported.

In this study, angle-resolved SXES measurements of B-K emission were conducted for  $Lu(Al,T)B_4$  ( $T=Cr, Fe, Mn, Mo$ ) single crystals to investigate the anisotropy of the chemical bonding state of the valence band and its dependence on the introduced  $T$  elements.

## 2 Experiment

For SXES measurements, an Electron Probe Micro Analyzer (EPMA, JXA-8230, JEOL) with an SXES system (SS-94000SXES, JEOL) was used [24]. Measurements were carried out at an acceleration voltage of 5 kV and a beam current of  $1.0 \times 10^{-7}$  A. The acquisition time for each spectrum was 30 sec $\times$ 30 times = 15 min. In this experiment, a varied line-spacing grating (JS200N) with an average groove density of 1200 lines/mm

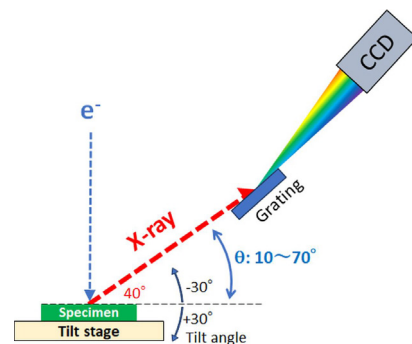
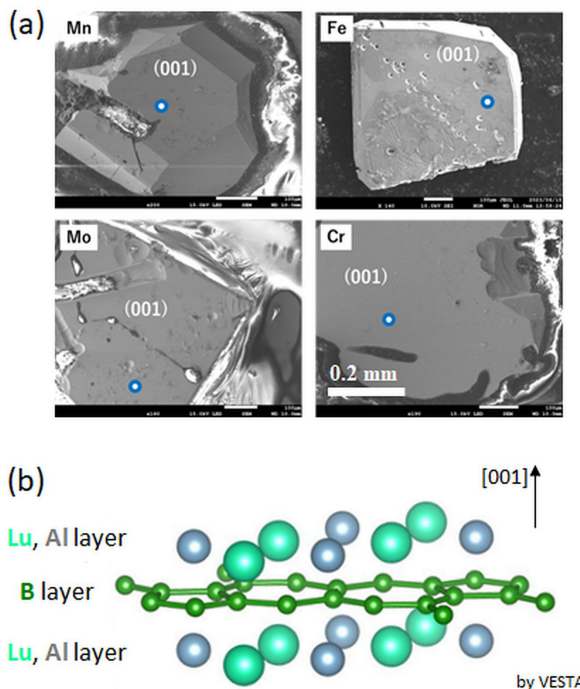


Fig. 1. Specimen tilt-stage for EPMA-SXES.

was used having the measurement range of 52-213 eV. The energy resolution of the spectrograph is 0.1 eV for the Al L-emission spectrum. To realize angle-resolved SXES measurements in the EPMA, an original specimen tilting stage was designed and manufactured [9]. The tilting stage can tilt the sample within  $\pm 30^\circ$  from horizontal setting, as shown in Fig. 1. A stepping motor can control the tilt angle by  $0.2^\circ$  steps. The acceptance angle of the spectrometer is  $\pm 0.3^\circ$ . The *c*-facets of  $\text{Lu}(\text{Al}, T)\text{B}_4$  single crystalline specimens were set parallel to the specimen stage. In this case, the X-ray emission spectrometer measures X-rays emitted in the  $40^\circ \pm 0.3^\circ$  direction from the *c*-plane, horizontal direction. Therefore, measurements in the X-ray emission angle range of  $q = 10^\circ \sim 70^\circ$  from the *c*-plane were able to be performed.

Single crystal specimens of  $\text{Lu}(\text{Al}_{1-x}\text{T}_x)\text{B}_4$  ( $T = \text{Cr, Fe, Mn, Mo}$ ) were prepared using the Al-self flux method [20,21]. The produced materials were examined by XRD to confirm the presence of  $\text{Lu}(\text{Al}_{1-x}\text{T}_x)\text{B}_4$  crystals and evaluate the lattice constants. The composition was evaluated by EPMA. Figure 2(a) shows SEM images of  $\text{Lu}(\text{Al}_{1-x}\text{T}_x)\text{B}_4$  ( $T = \text{Cr, Fe, Mn, Mo}$ ) specimens with a (001) facet. EDS analyses of the specimens in Fig. 2(a) showed Al:T were 1:1-0.6, which roughly agrees with the result of EPMA analysis [20]. B K-emission spectra were obtained from the dotted areas of about 1 mm in diameter in the images. Figure 2(b) shows a schematic figure of the crystal structure of non-doped  $\text{LuAlB}_4$  [25]. Doped *T* elements presumably occupy Al-sites randomly. However, the structure refinement analysis of the produced materials has not been done.

Since B K-emission is related to electron transitions from the VB to 1s core-state under the dipole transition condition, the obtained spectrum intensity profile could be compared with density of states (DOS) of *p*-symmetry of the VB. Unfortunately, since the crystal structure refinement analysis has not been performed for the present crystals, the B-K spectrum intensity profile could be compared only with theoretically calculated results for the non-doped  $\text{LuAlB}_4$ . For the calculation, WIEN2k code was employed using the full-potential linear extended plane-wave method [26]. The exchange-correlation function was applied using the generalized gradient approximation formulated by Perdew, Bruke and Ernzerhof



**Fig. 2.** (a) SEM images of crystalline specimens with (001) facet. Dots positions were examined by SXES. (b) Crystal structure of  $\text{LuAlB}_4$  [25].

[27]. The end conditions for the self-consistent cycle calculation were set to a convergence-energy of 0.0001 Ry, a force of 0.001 Ry/au and a charge of 0.001e.

### 3 Results and discussion

Figure 3(a) shows a B-K emission spectrum of Lu(Al,Mn)B<sub>4</sub> in an energy range of 176–188 eV. Since this emission is due to the dipole electric transitions, the intensity distribution corresponds to the B-2*p* DOS of the VB. A vertical arrow positioned at the high energy end of the spectrum intensity distribution, corresponds to the upper end of the VB. The spectrum shows three structures as indicated by vertical lines. Figure 3(b) shows the B-2*p* DOS of LuAlB<sub>4</sub> obtained from *ab initio* calculations. Since the present materials have two-dimensional B-layers, the B-K emission intensity  $I(\theta)$  at a take-off angle  $\theta$  from *c*-plane could be written as  $I(\theta) = \cos^2\theta \times I_{pz} + 1/2(1 + \sin^2\theta) \times I_{px+py}$  as in the case of *h*-BN [8]. Thus, the DOS is broken down into *px+py* and *pz* components. It can be seen that the *pz* component is larger than the *px+py* component at the top region of the VB, suggesting a p-character orbital. For comparison, those spectra were aligned so that the structures at 181 eV and 183 eV of the measured B-K

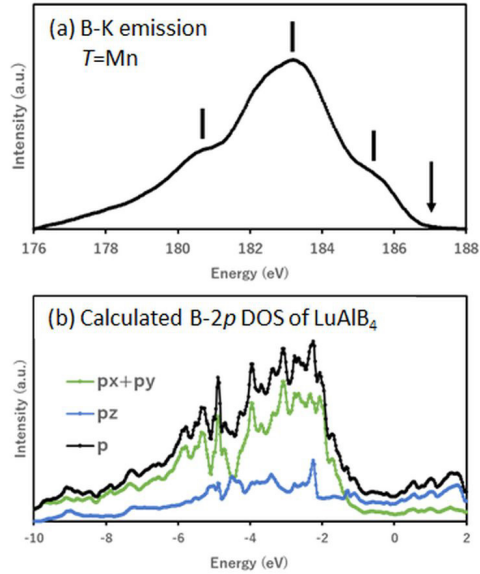


**Fig. 3.** (a) B-K emission spectrum (1st order) of *T*=Mn specimen. (b) Calculated B-2*p* DOS of non-doped LuAlB<sub>4</sub>.

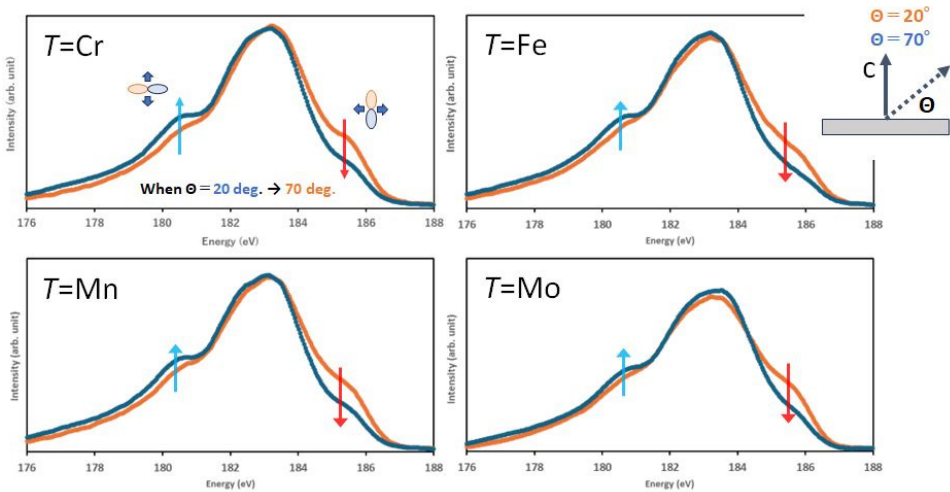


**Fig. 4.** B-K emission spectra of Lu(Al,*T*)B<sub>4</sub> (*T*= Cr, Mn, Fe, Mo) obtained at  $q = 20^\circ$  and  $70^\circ$ . Each spectrum was normalized by each integrated intensity. Arrows indicate the intensity change when  $q$  changed from  $20^\circ$  and  $70^\circ$ .

emission spectrum match with the calculated DOS peaks. Since the calculated result is for the non-doped LuAlB<sub>4</sub>, a rigorous comparison cannot be made. However, a correspondence between the structures around 181 and 183 eV in the observed and calculated structures is noticeable.

Figure 4 shows the B K-emission spectra of Lu(Al,*T*)B<sub>4</sub> (*T*= Cr, Fe, Mn, Mo) obtained at take-off angles of  $q=20^\circ$  and  $70^\circ$ . The spectral intensity distributions were normalised by their integrated intensities from 174 eV to 188 eV. It can be seen that the presence of the three structures indicated by vertical lines in Fig. 3(a) are similar for the four spectra. Thus, the difference of electronic structure due to doping atoms is not apparent for the B-2*p* DOS of the VB. The angle dependence of the structures at the top of the VB (185-187 eV) and at the bottom of the VB (179-181 eV) can be explained by referring to the angle dependence of the graphite C-K emission spectra (2<sup>nd</sup> order) shown in Fig. 5. The top of the B-K of Lu(Al,*T*)B<sub>4</sub> shows a larger intensity for the smaller take-off angle of  $q=20^\circ$ . This means the bonding charge at the top of the VB distributes out of the 2D B-layer (parallel to *c*-axis), p-character. On the other hand, the bottom region of the B-K shows a larger intensity for the larger take-off angle of  $q=70^\circ$ , suggests the bonding charge distributes in the 2D B-layer, s-character. The tendency of p and s-bonding character, respectively, in the top and the bottom of the VB seems common for 2D layered materials. On the other hand, the middle of the VB (182-184 eV) of the dominant peak intensity region shows less angle dependence, suggesting the bonding charge distributes isotropically. Those characters of the angle dependence in the top and bottom regions of the VB and the almost no angle dependence in the middle of the VB are common for the materials examined. As a whole, the anisotropy of the bonding charge distribution of 2D B-layer in Lu(Al,*T*)B<sub>4</sub> exists but smaller than that of graphite and *h*-BN. This rather isotropic distribution of the bonding charge can contribute to form inter-layer bonds and the hardness of the bulk materials.

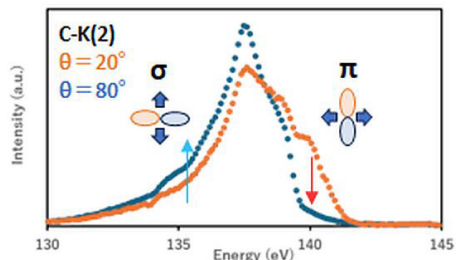


**Fig. 5.** C-K emission spectra (2<sup>nd</sup> order) of graphite taken at  $q=20^\circ$  and  $80^\circ$ . Top region corresponds to p-character. Middle (peak area) and bottom region correspond to s-character.

The spectroscopic character dependence on element *T* was observed in the peak energy of B-K emission spectra. The peak energy of the specimen of *T*= Mo is a little larger than those of *T*= Cr, Fe, Mn specimens by 0.3 eV. This peak shift could be due to the chemical shift of B K-shell energy level to the larger binding energy side by 0.3 eV, suggesting a smaller amount of valence charge associated with B in the *T*=Mo specimen than that in the *T*=Cr, Fe, Mn specimens. This can be understood by the larger electronegativity of Mo atom than that of Cr, Fe, Mn.

## 4 Conclusions

In this study, angle-resolved SXES measurements were performed for Lu(Al,*T*)B<sub>4</sub> (*T*= Cr, Mn, Fe, Mo) single crystals. The B-K emission spectra of the materials studied show angle

dependences in the top (p-character) and bottom (s-character) regions, but almost no angle dependence in the middle of the VB. Those trends were common for the four materials. As a whole, the anisotropy in the bonding charge distribution of the 2D boron-layer in Lu(Al,T)B<sub>4</sub> is much smaller than that of graphite and *h*-BN. The almost no angle-dependence, isotropic charge distribution, can contribute to form the inter-layer bonding between B-layer and adjacent Lu(Al,T) layers. To confirm the relation between the bonding nature and the physical properties of the bulk materials, crystal structure refinement and calculations based on the structure data should be done in the next step.

## References

1. D.J. Fabian, L.M. Watson and C.A.W. Marshall, Soft x ray spectroscopy and the electronic structure of solids. *Rep. Prog. Phys.* **34** 601-696 (1972).  
DOI 10.1088/0034-4885/34/2/304
2. M. Terauchi, Valence electron spectroscopy for transmission electron microscopy. In: *Characterization Tools for Nanoscience & Nanotechnology*, ed. Kumar C S S R, pp. 287-331 (Springer-Verlag Berlin Heidelberg, 2014).
3. M. Terauchi, T. Imazono and M. Koike, Chemical State Analysis with Soft-X-ray Emission Spectroscopy Based on SEM. (in Japanese) *Journal of The Surface Science Society of Japan* **36** 184-188 (2013).
4. R. Kasada, Y. Ha, T. Higuchi and K. Sakamoto, Degrade B<sub>4</sub>C Control Rod Investigated with Soft X-ray Emission Spectrometer in Electron Probe Micro-analysis. <https://doi.org/10.1038/srep25700>  
<https://www.nature.com/articles/srep25700>
5. S. Ishii, M. Terauchi, Y. Sato, N. Tamaru, M. Aono and H. Abe, Soft X-ray emission spectroscopy study of characteristic bonding states and its distribution of amorphous carbon–nitride (a-CN<sub>x</sub>) films. *Microscopy* **67** 244–249 (2018).  
<https://doi.org/10.1093/jmicro/dfy024>
6. M. Terauchi, Y.K. Sato and M. Takeda, Chemical state mapping of *p/n*-controlled SrB<sub>6</sub> bulk specimens by soft X-ray emission electron microscope. *Applied Science* **11** 9588-1-9588-9 (2021).  
<https://doi.org/10.3390/app11209588>
7. W. Heitler, *The Quantum Theory of Radiation*, 3rd ed. (Dover Publication, New York, 1954).
8. C.E. Tegeler, N. Kosuch, G. Wiech and A. Faessler, Anisotropic Emission of the X-Ray K-Emission Band of Nitrogen in Hexagonal Boron Nitride. *phys. stat. sol. (b)* **84** 561-567 (1977).  
<https://doi.org/10.1002/pssb.2220840219>
9. R. Ebisu, Y.K. Sato, T. Yamada and M. Terauchi, Anisotropic electronic structure of NaAlSi studied by angle-resolved soft x-ray emission spectroscopy. *J. Appl. Phys.* **134** 215107-1-215107-8 (2023).  
<https://doi.org/10.1063/5.0178436>
10. Y. Hada, M. Terauchi, T. Saito, Y.K. Sato, M. Baba and M. Takeda, Anisotropic electronic structure study of MgB<sub>2</sub>C<sub>2</sub> using soft X-ray emission spectroscopy microscopes. *Microscopy* **74** 86-91 (2024).

- <https://doi.org/10.1093/jmicro/dfae048>
11. B. Albert and H. Hillebrecht, Boron: Elementary Challenge for Experimenters and Theoreticians. *Angewandte Chemie* **48** 8640-8668 (2009).  
<https://doi.org/10.1002/anie.200903246>
  12. J. Nagamatsu, N. Nakagawa, T. Muranaka, Y. Zenitani and J. Akimitsu, Superconductivity at 39 K in magnesium diboride. *Nature* **410** 63-64 (2001).  
<https://www.nature.com/articles/35065039#citeas>
  13. M. Sawada, J. Shimoyama, N. Takagi, T. Motoki, M. Kodama and H. Tanaka, A new carbon source of  $MgB_2C_2$  for the synthesis of carbon-doped  $MgB_2$ . *Solid State Comm.* **281** 53-56 (2018).  
<https://doi.org/10.1016/j.ssc.2018.06.011>
  14. M. Worle and R. Nesper,  $MgB_2C_2$ , a new graphite-related refractory compound. *J. Alloys and Compounds* **216** 75-83 (1994).  
[https://doi.org/10.1016/0925-8388\(94\)91045-6](https://doi.org/10.1016/0925-8388(94)91045-6)
  15. P. Rogl and L. Delong, New Ternary Transition Metal Borides Containing Uranium and Rare Earth Elements. *J. Less-Common Metals* **91** 97-106 (1983).  
[https://doi.org/10.1016/0022-5088\(83\)90099-1](https://doi.org/10.1016/0022-5088(83)90099-1)
  16. S. Okada, T. Shishido, T. Mori, K. Kudou, K. Iizumi, T. Lundström and K. Nakajima, Properties of  $REAlB_4$  and  $Lu_2AlB_6$  crystals grown from RE-Al-B (RE = Tm, Yb, Lu) melts. *J. Alloys and Compounds* **408-412** 547-550 (2006).  
<https://doi.org/10.1016/j.jallcom.2005.01.078>
  17. T. Mori, I. Kuzmych-Ianchuk, K. Yubuta, T. Shishido, S. Okada, K. Kodou and Y. Grin, Direct elucidation of the effect of building defects on the physical properties of  $\alpha$ -TmAlB<sub>4</sub>; An AlB<sub>2</sub>-type analogous “tiling” compound. *J. Appl. Phys.* **111** 07E127-1-07E127-3 (2012).  
<https://doi.org/10.1063/1.3674285>
  18. X.J. Wang, T. Mori, I. Kuzmych-Ianchuk, Y. Michiue, K. Yubuta, T. Shishido, Y. Grin, S. Okada and D.G. Cahill, Thermal conductivity of layered borides: The effect of building defects on the thermal conductivity of TmAlB<sub>4</sub> and the anisotropic thermal conductivity of AlB<sub>2</sub>. *APL Materials* **2** 046113-1-046113-6 (2014).  
<https://doi.org/10.1063/1.4871797>
  19. H. Takaki, K. Kobayashi, M. Shimono, N. Kobayashi, K. Hirose, N. Tsujii and T. Mori, Thermoelectric properties of a magnetic semiconductor CuFeS<sub>2</sub>. *Materials Today Physics* **3** 85-92 (2017).  
<https://doi.org/10.1016/j.mtphys.2017.12.006>
  20. K. Kouzu, T. Yamasaki, S. Okada, T. Mori, Q. Guo, T. Shishido, K. Yubuta, A. Nomura, A. Yoshikawa and P. Rogl, Crystal Growth and Physical Properties of  $Lu(Al_{1-x}T_x)B_4$  ( $T = Fe, Cr$ ) by Al-Self Flux. *Solid State Phenomena* **289** 120-126 (2019).  
<https://doi.org/10.4028/www.scientific.net/SSP.289.120>
  21. K. Kouzu, S. Okada, T. Hagiwara, A. Nomura, T. Shishido, A. Yoshikawa, K. Yubuta and T. Mori, Syntheses and physical properties of  $Lu(Al, T)B_4$  ( $T = Cr, Fe, Mo, Mn$ ) compounds. *Abstract of JSBB 2023* (in Japanese): PS15 (2023).
  22. K. Kouzu, T. Yamasaki, S. Okada, T. Mori, Q. Guo, K. Yubuta, A. Nomura, T. Shishido, A. Yoshikawa and P. Rogl, Syntheses and Properties of  $Yb(Al_{1-x}T_x)B_4$  ( $T = Cr, Fe$ ) Compounds. *J. Jpn. Soc. Powder Metallurgy* **66** 525-529 (2019).

- <https://doi.org/10.2497/jjspm.66.525>
23. K. Kouzu, S. Okada, T. Hagiwara, A. Nomura, K. Yubuta, T. Mori, T. Shishido and A. Yoshikawa, Syntheses and some properties of solid solution  $\text{Yb}(\text{Al}, T)\text{B}_4$  ( $T = \text{Mo}$  or  $\text{W}$ ) compounds. *Solid State Sciences* **158** 107735-1-107735-5 (2024).  
<https://doi.org/10.1016/j.solidstatesciences.2024.107735>
  24. H. Takahashi, N. Handa, T. Murano, M. Terauchi, M. Koike, T. Kawachi, T. Imazono, N. Hasegawa, M. Koeda, T. Nagano, H. Sasai, Y. Oue, Z. Yonezawa and S. Kuramoto, Exciting Possibilities of Soft X-ray Emission Spectroscopy as Chemical State Analysis in EPMA and FESEM. *Microscopy and Microanalysis* **20(suppl. 3)** 684-685 (2014).  
doi:10.1017/S1431927614005145
  25. R.T. Macaluso, S. Nakatsuji, K. Kuga, E.L. Thomas, Y. Machida, Y. Maeno, Z. Fisk and J.Y. Chan, Crystal Structure and Physical Properties of Polymorphs of  $\text{LnAlB}_4$  ( $\text{Ln} = \text{Yb}, \text{Lu}$ ). *Chem. Mater.* **19** 1918-1922 (2007).  
<https://doi.org/10.1021/cm062244+>
  26. P. Blaha, K. Schwarz, F. Tran, R. Laskowski, G.K. Madsen and L.D. Marks, WIEN2k: An APW+lo program for calculating the properties of solids. *J. Chem. Phys.* **152** 074101-1-074101-30 (2020).  
<https://doi.org/10.1063/1.5143061>
  27. J.P. Perdew, K. Burke and M. Ernzerhof, Generalized Gradient Approximation Made Simple. *Phys. Rev. Lett.* **77** 3865-3868 (1996).  
<https://doi.org/10.1103/PhysRevLett.77.3865>